Unstructured Direct Ink Write 3D Printing of Functional Structures with Ambient Temperature Curing Dual-Network Thermoset Ink

Connor D. Armstrong, Liang Yue, Frédéric Demoly, Kun Zhou, H. Jerry Qi

▶ **To cite this version:**

Connor D. Armstrong, Liang Yue, Frédéric Demoly, Kun Zhou, H. Jerry Qi. Unstructured Direct Ink Write 3D Printing of Functional Structures with Ambient Temperature Curing Dual-Network Thermoset Ink. Advanced Intelligent Systems, 2022, 5 (1), pp.2200226. ⟨10.1002/aisy.202200226⟩. ⟨hal-05455032⟩

HAL Id: hal-05455032

https://hal.science/hal-05455032v1

Submitted on 12 Jan 2026

HAL is a multi-disciplinary open access archive for the deposit and dissemination of scientific research documents, whether they are published or not. The documents may come from teaching and research institutions in France or abroad, or from public or private research centers.

L'archive ouverte pluridisciplinaire **HAL**, est destinée au dépôt et à la diffusion de documents scientifiques de niveau recherche, publiés ou non, émanant des établissements d'enseignement et de recherche français ou étrangers, des laboratoires publics ou privés.

Distributed under a Creative Commons CC BY 4.0 - Attribution - International License

ADVANCED INTELLIGENT SYSTEMS
Open Access
www.advintellsyst.com

Unstructured Direct Ink Write 3D Printing of Functional Structures with Ambient Temperature Curing Dual-Network Thermoset Ink

*Connor D. Armstrong, Liang Yue, Frédéric Demoly, Kun Zhou, and H. Jerry Qi**

Fabrication of structures in unstructured environments is a promising field to expand the application spaces of additive manufacturing (AM). One potential application is to add new components directly onto existing structures. Herein, a versatile, reconfigurable direct ink writing (DIW) manufacturing method is developed in tandem with a two-stage hybrid ink designed to fabricate high-strength, self-supporting parts in unconventional printing spaces such as underneath a build surface or horizontally. This two-stage hybrid DIW ink combines a photopolymer and a tough epoxy resin. The photopolymer can cure rapidly to enable layer-by-layer printing of complex structures. It also possesses adequate adhesion to allow the fabrication of large volume structures on a diversity of substrates including acrylic, wood, glass, aluminum, and concrete. The epoxy component can cure after 72 h in ambient conditions with further increased adhesion strengths. The capabilities of the reconfigurable DIW extrusion nozzle method to print complex structures in inverted and horizontal environments are demonstrated. Finally, via addition of DIW-deposited conductive paths, a functional 3D-printed structure capable of in situ deformation monitoring is created. This work has the potential to be used for applications such as appending new parts to existing structures for increasing functionality, repair, and structure health monitoring.

1. Introduction

Extrusion-based additive manufacturing (AM) such as fused filament fabrication (FFF) and direct ink writing (DIW) are popular choices for 3D printing due to their low cost, simplicity, open framework, and broad material versatility. In recent years, researchers have aimed to broaden potential applications of extrusion-based AM by modifying build hardware, control schemes, and layer structure.[1–4] Furthermore, researchers have also utilized DIW material versatility to create structures with a vast breadth of properties ranging from elastomeric and viscoelastic to high-strength rigid.[5–11] As a result, developing novel AM techniques in tandem with ink feedstock with tuned mechanical characteristics to create application-specific methods has been of great interest.[12–22]

An emerging application of AM is to fabricate new components directly onto existing structures, which can have unstructured surfaces unsuitable for conventional DIW 3D printing. This includes applications where the existing build surface is either too large or sensitive to be moved such as in situ construction repair and in vivo bone and tissue repair.[23–25] However, conventional extrusion-based techniques deposit layers on the *XY* plane with a downward-facing extrusion nozzle and build parts upward.[26] Due to the limited printing space, 3D-printed parts are then removed from the tray to be assembled with others. Thus, the ability to create parts in an unstructured manufacturing space with these conventional techniques is limited. Fabricating on unconventional and nonplanar surfaces has been explored via both redefining motion of the build plate and/or extrusion head.[27–29] Yet, while previous studies have successfully created geometries unattainable with conventional AM methods using a moving build plate, this approach is unsuitable for printing onto an existing, fixed build surface.[30,31]

C. D. Armstrong, L. Yue, H. J. Qi
The George W. Woodruff School of Mechanical Engineering
Georgia Institute of Technology
Atlanta, GA 30332, USA
E-mail: qih@me.gatech.edu

The ORCID identification number(s) for the author(s) of this article can be found under https://doi.org/10.1002/aisy.202200226.

© 2022 The Authors. Advanced Intelligent Systems published by Wiley-VCH GmbH. This is an open access article under the terms of the Creative Commons Attribution License, which permits use, distribution and reproduction in any medium, provided the original work is properly cited.

DOI: 10.1002/aisy.202200226

C. D. Armstrong, H. J. Qi
Renewable Bioproducts Institute
Georgia Institute of Technology
Atlanta, GA 30332, USA

F. Demoly
ICB UMR 6303 CNRS
University of Bourgogne Franche-Comté, UTBM
90010 Belfort, France

K. Zhou
Singapore Centre for 3D Printing
School of Mechanical and Aerospace Engineering
Nanyang Technological University
50 Nanyang Avenue, Singapore 639798, Singapore

Furthermore, studies utilizing movement of the extrusion head predominantly used FFF to deposit rapidly solidifying thermoplastics rather than DIW. This can be attributed to the sensitivity to gravitational effects on the viscoelastic, shear-thinning DIW inks requiring the extrusion nozzle to be facing downward during deposition, at the cost of impeding formable geometries.[32] To overcome this barrier, a rapidly solidifying DIW ink must be utilized. To achieve this, researchers have investigated inks with polymer networks catalyzed via continuous ultraviolet (UV) irradiation.[33,34] Moreover, to further preserve shape integrity and improve properties, researchers have developed multi-stage curing inks that typically consist of a photopolymer and a thermal cure resin.[35] However, secondary thermal curing requires placing the printed structure in an oven, which is impossible if the application is to print an object on an existing structure.

In this work, we introduce a novel DIW technique for manufacturing parts in nontraditional environments whereby the extrusion nozzle is repositioned to facilitate the fabrication of parts in unstructured manufacturing spaces, such as underneath the build surface or horizontally (**Figure 1**a and S1a,b, Supporting Information). Parts were created using a two-stage photo-epoxy thermoset resin wherein the acrylate-based photo resin enabled rapid shape forming while the epoxy resin developed a high-strength network highly compatible with the photo-cured polymer network at room temperature (Figure 1b,c). We investigated various ratios of photo cure and epoxy monomer constituents of the two-stage resin on mechanical characteristics to determine the ideal balance of strength and rapid polymerization. The tough epoxy resin constituent of printed ink rose to 50% of the degree of conversion (DoC) after 24 h, increasing further to 73.2% after 48 h, and finally achieving 86.3% after 72 h in ambient and room-temperature conditions. Due to the photo-epoxy two-stage curing resin's ability to form an interpenetrating polymer network, the fully cured printed structures demonstrated a high bonding affinity to a variety of substrates. With a favorable photo-to-epoxy resin ratio, we then demonstrated the capabilities of this technique via 3D printing of several structures under a build platform, including a bio-inspired "beehive," conical structures with large overhangs, and load-bearing arches (Figure 1c). Similarly, horizontal parts were printed via reconfiguring the DIW extrusion nozzle such that the direction ink deposition was parallel to the *XY* plane whereby structures could be fabricated on a vertical surface. As a demonstration, we printed a zero-support horizontal beam with integrated conductive elements to enable in situ deformation sensing.

2. Experimental Section

2.1. Two-Stage Resin Preparation

The two-stage curing resin consisted of varying ratios of photopolymer resin and epoxy resin (Figure 1a–c). A detailed breakdown of chemical constituents can be found in **Table 1**. The monomers for the photopolymer resin component consisted of 95 wt% ethoxylated trimethylolpropane triacrylate (TMPTA) monomer (Sigma-Aldrich, St. Louis, MO, USA) and 5 wt% glycidyl methacrylate (GMA) (Sigma-Aldrich) as a reactive diluent. The monomers for the epoxy resin contained a 100:32 ratio of Epon 828 (difunctional bisphenol A/epichlorohydrin (DGEBA); Hexion, Columbus, OH, USA) and Jeffamine D230 curing agent (O,O′-Bis(2-aminopropyl) polypropylene glycol-block-polyethylene glycol-blockpolypropylene glycol) (Sigma-Aldrich). The photocuring and epoxy resins were separately hand mixed, and then the resins were combined to form the two-stage resin, followed by 5 min of magnetic stirring to further homogenize the mixture. 1 wt% photoinitiator Irgacure 819 (Bis(2,4,6-trimethylbenzoyl)-phenylphosphineoxide) (Sigma-Aldrich) and 3 wt% co-curing agents were added to the two-stage resin mixture to facilitate photopolymerization and catalyze room-temperature curing, respectively. The co-curing agent consisted of 70 wt% triethanolamine, 20 wt% piperazine, and 10 wt% *N*-aminoethylpiperazine (Sigma-Aldrich). Finally, 7 wt% fumed silica

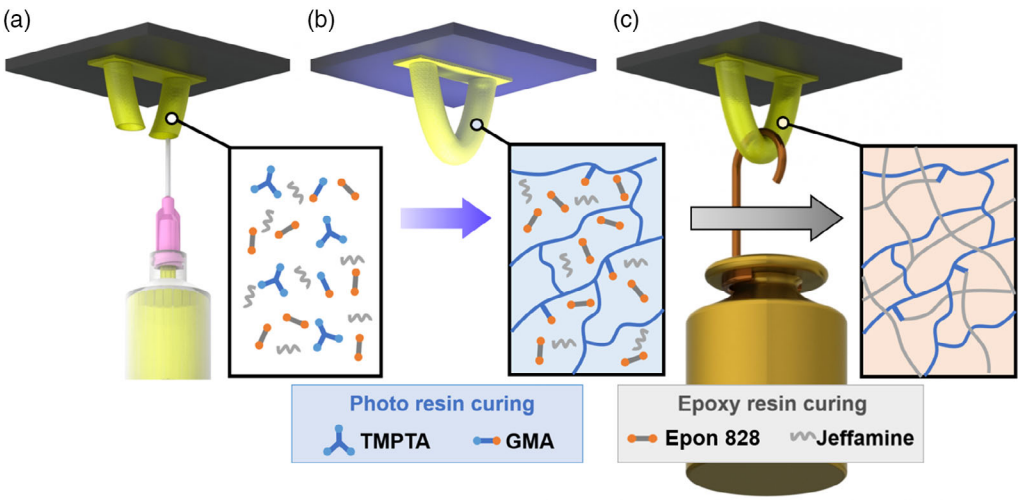

Figure 1. Graphical depiction of the inverted direct ink writing (DIW) additive manufacturing (AM) procedure fabricating an arch structure under the printing platform. a) Layer deposition of uncured two-stage resin ink onto the structure. b) Solidification of a deposited layer via the development of a photopolymer network facilitated by UV radiation. c) Strengthening of printed structure through the development of an interpenetrating polymer network via autonomous ambient temperature conversion of epoxy resin.

© 2022 The Authors. Advanced Intelligent Systems published by Wiley-VCH GmbH

Table 1. Chemical ingredients of the two-stage resin.

Chemical		Structure	Function	% of Total	wt%
Photo cure resin	TMPTA	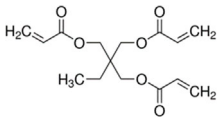	Acrylate monomer	*x*	95%
	GMA	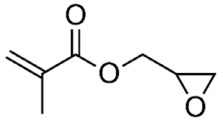	Reactive dilutant		5%
	Irgacure 819	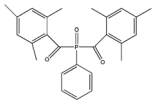	Photoinitiator	1%	
Epoxy resin	Epon 828	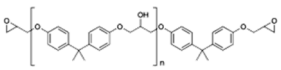	Epoxy oligomer	1−*x*%	75.75%
	Jeffamine D230	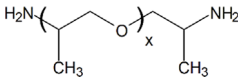	Curing agent		25.25%
	Triethanolamine	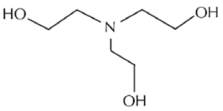	Co-curing agent	3%	70%
	Piperazine	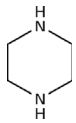	Co-curing agent		20%
	N-aminoethylpiperazine	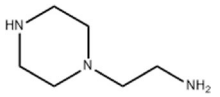	Co-curing agent		10%

(Sigma-Aldrich) was mixed into the liquid two-stage resin to enable shear-thinning behavior required for DIW 3D printing. Due to the co-curing agent's ability to catalyze epoxy resin at room temperature, the working life of the two-stage ink was around four hours.

Several different compositions of the two-stage curing resin were created with varying ratios of photopolymer resin and epoxy resin: 70:30, 50:50, 30:70 wt% (denoted as PE30, PE50, and PE70, respectively). Additionally, inks containing purely photopolymer resin and purely epoxy resin (100:0, 0:100) were created (denoted as P and E, respectively).

Once prepared, the two-stage resin was loaded into syringes and centrifuged for 20 min to completely remove air bubbles, then mounted to a custom-built DIW printer.[36] The DIW printer uses compressed air delivered by an Ultimus V air pressure controller (Nordson EFD, East Providence, RI, USA) to extrude the created ink through a tapered deposition nozzle (Figure 1a).

Additionally, a conductive DIW ink was prepared with ME603 conductor paste (DuPont, Wilmington, DE, USA) combined with 3 wt% Timical Super C45 carbon black (MTI Corporation, Richmond, CA, USA) to improve conductivity and aid in shape retention post-extrusion.[37]

2.2. Sample Preparation and Material Characterization

To characterize the properties of the two-stage resins, tensile, dynamic mechanical analysis (DMA), Fourier transform infrared spectroscopy (FTIR), and rheological tests were performed. Dogbone-style samples for tensile and DMA characterization experiments were cast in a silicone/polydimethylsiloxane (PDMS) mold. Samples with varying resin compositions (P, PE30, PE50, PE70, E) were subjected to a 60 s UV curing (intensity = 66 mW cm^{-2}) followed by a 72 h room temperature cure. Additionally, PE70 tensile samples were subjected to only UV curing for 1, 15, 30, and 60 s. FTIR and rheological experiments were conducted using only PE70 resin.

To characterize the mechanical properties of the two-stage resin at various resin composition ratios (P, PE30, PE50, PE70, E), tensile tests ($n = 3$) were performed using a universal mechanical testing machine (Criterion, MTS, Eden Prairie, MN, USA) to acquire Young's modulus (E) as well as yield and ultimate engineering stresses and strains. Furthermore, tensile tests of PE70 resin samples subjected to 66 mW cm^{-2} UV irradiation for 1, 15, 30, and 60 s were performed. Additionally, DMA tests using a DMA tester (Q800, TA Instruments, New Castle, DE, USA) were carried out to obtain the glass transition temperature

© 2022 The Authors. Advanced Intelligent Systems published by Wiley-VCH GmbH

(T_g), storage (E') and loss (E") moduli, and tanδ of the two-stage resin. Rheological measurements of PE70 two-stage resin were obtained at room temperature using an ARES G2 rotating rheometer (TA Instruments). Viscosity (η), shear storage (G'), and loss moduli (G") were obtained over a range of shear rates (0.1–200 1/s). Finally, two sets of FTIR experiments were performed to determine the DoC for both photopolymerization and room-temperature epoxy cure reactions in PE70 resin. For photopolymerization, FTIR scans were taken on resin samples subjected to 66 mW cm^{-2} UV irradiation for (0, 1, 3, 5, 7, 15, 30, and 60 s). Likewise—for the room-temperature epoxy cure—FTIR scans were performed on fully photopolymerized PE70 samples 0, 12, 24, 36, 48, and 72 h after creation.

To understand the bonding strength of printed structures, $5 \times 10 \times 20$ mm pillars were printed onto acrylic, wood, glass, aluminum, and concrete substrates. Substrates with pillars directly after printing (0 h) as well as after 72 h were constrained to a plate affixed to a universal mechanical testing machine (Criterion, MTS). Next, the pillars were constrained in a tensile test grip and a load was applied until the pillar delaminated from the substrate. The critical stress measured was determined to be the adhesion strength.

2.3. 3D Printing of Structures

3D models were prepared using SolidWorks (Dassault Systèmes SE, Vélizy-Villacoublay, France) computer-aided design (CAD) software. Prior to 3D printing, the models were imported into the computer-aided manufacturing (CAM) software, Repetier (Hot-World GmbH & Co. KG, Willich in North Rhine-Westphalia, Germany), for slicing into discrete layers. The resulting toolpath control code (gcode) was modified using custom MATLAB (MathWorks, Natick, MA, USA) scripts to redefine the position axis such that the extrusion head would move downward on the *Z*-axis, and along the *Y*-axis for horizontal prints for each layer. Structures were subsequently printed through a 0.58 mm diameter nozzle onto glass substrates at a printing speed of 10 mm s^{-1} and extrusion pressure of 75 kPa. UV irradiation (66 mW cm^{-2}, 15 s) was applied to every alternating layer. The conductive paths were printed through a 0.41 mm diameter nozzle at a printing speed of 10 mm s^{-1} and extrusion pressure of 190 kPa.

3. Results and Discussion

3.1. Mechanical and Material Characterization

DMA of thermally cured samples over the range of 30–170 °C revealed that the two-stage resin has a T_g of 94.4, 121.2, 114.8, 97.4, and 91.5 °C for P, PE30, PE50, PE70, and E resin compositions, respectively, indicated by the peaks in tanδ curves (dashed lines) (**Figure 2**a). Importantly, the materials exhibit a single distinct T_g despite the varying concentrations of monomers in the photo and thermal resin constituents having different T_g values. This suggests that the photo and thermal cure networks are highly compatible due to epoxide groups presented in the reactive dilutant GMA component of the photopolymer resin, allowing for the epoxy resin component to form an interpenetrating network with the TMPTA photopolymer network with no macroscale phase separation between the two components. As photo resin concentration increases, the tanδ curves begin to exhibit fewer and less distinct peaks. As a result, the tanδ peak for P is comparably small in height, but very broad. This indicates there is a longer property transition compared to all other conditions, which can account for the P condition's deviation from the upward trend in T_g as photo resin concentration increases. Furthermore, based on the storage modulus behavior of P, it can be surmised this phenomenon is due to the highly crosslinked nature of the photo cure network as it has triacrylate monomers, and therefore has more crosslinking points. This high crosslink concentration inhibits movement of the interpenetrating polymer network, resulting in the observed increasing trend in T_g versus photo resin concentration.

The results of the tensile tests for each resin composition are presented in Figure 2b. The sole photopolymer resin (P) exhibits highly rigid, albeit low strength, behavior as evidenced by the comparably large Young's modulus versus other conditions (2.21 GPa) coupled with inferior tensile strength and fracture strain. However, increasing epoxy resin concentration resulted in an increase in the strength and ductility of the cured resins. Indeed, the addition of epoxy resin—even in the lowest concentration of PE30—affords a 170% increase in tensile strength versus the solely photopolymerized resin (23.6 ± 2.1 versus 63.5 ± 3.5 MPa). Moreover, the tensile strength of PE70 is comparable to that of the solely epoxy resin (81.4 ± 5.7 versus 79.5 ± 4.8 MPa), indicating that the epoxy network becomes the primary contributor to the strength of the material despite it only comprising 70 wt% epoxy. The increasing influence of the epoxy network over the rigid photo-cure network also manifests in a 0.18–0.32 GPa drop in Young's modulus versus P as epoxy concentration increases. Furthermore, increasing epoxy resin concentrations leads to a linear increase in fracture strain from 1.4 for P to 6.6% PE70 ($R^2 = 0.93$). However, despite PE70 and E having comparable tensile strengths, there is a relatively large discrepancy in fracture strain increase from PE70 to E ($\Delta\varepsilon = 2.7\%$). This implies that, despite the strength of the epoxy network, the highly crosslinked—and therefore rigid—photo-cure acrylate network impedes the deformation of the interpenetrating two-stage network.

Furthermore, we performed FTIR experiments to understand the curing kinetics of both the photo cure and epoxy resin networks, DoC with respect to time is presented in Figure 2c,d for photo cure and photo epoxy resin networks, respectively. DoC for both resin constituents was determined through analysis of the absorbance intensity of selected wavenumbers corresponding to bonds which drop in frequency as the respective polymer networks develop (Figure S2a,b, Supporting Information). Because our inverted and horizontally printed structures are significantly impacted by gravitational forces, a rapidly solidifying material is essential for parts to maintain their structure. As previously discussed, the high presence of bonding sites of the triacrylate TMPTA monomer allows for rapid polymerization, and therefore the development of a suitably stable/solidified network for the purpose of self-support. When exposed to UV irradiation with a light intensity of 66 mW cm^{-2} for one second, the photopolymer network constituent began rapidly developing (42.5% DoC)—and therefore solidifying—with a Young's

© 2022 The Authors. Advanced Intelligent Systems published by Wiley-VCH GmbH

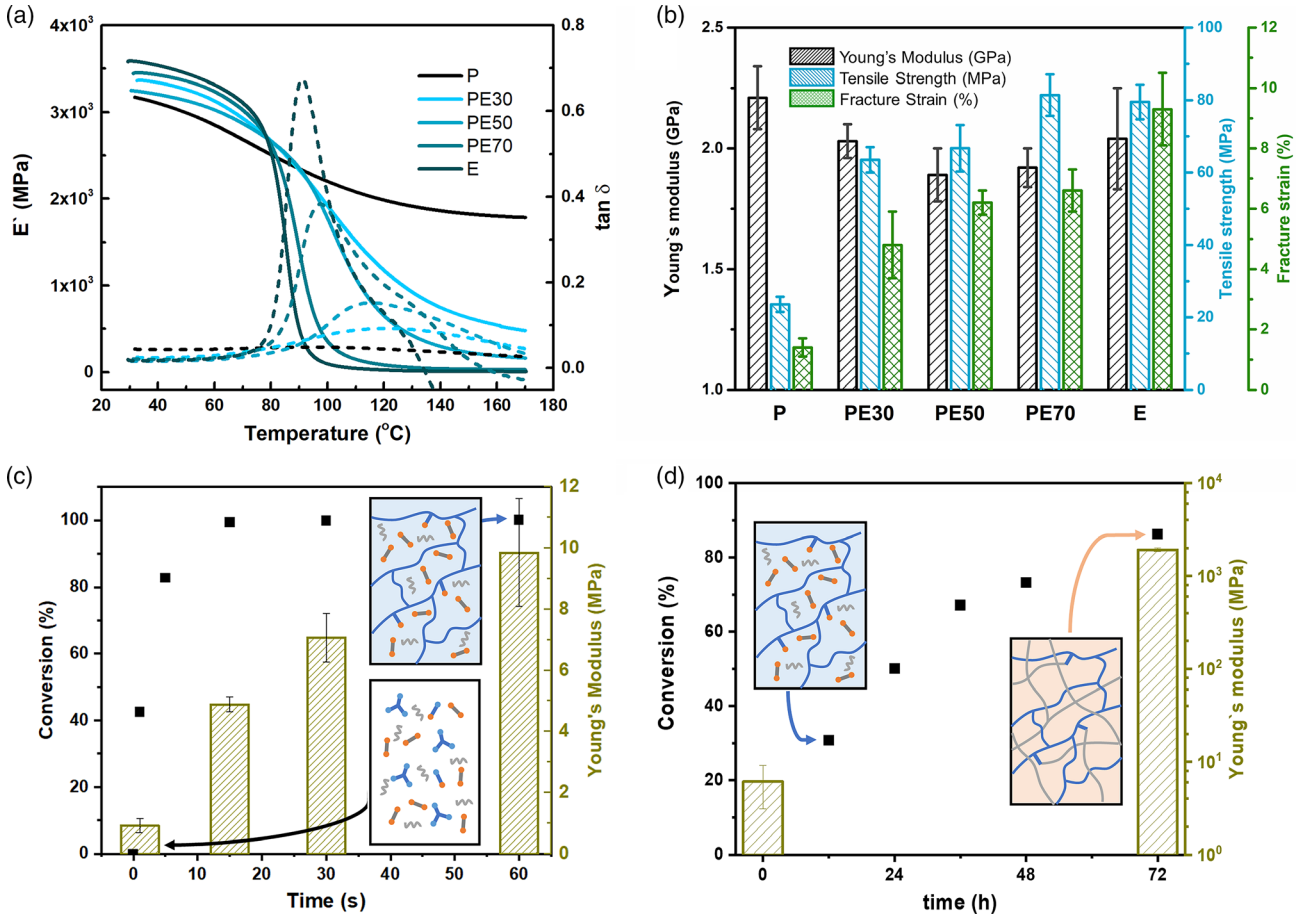

Figure 2. Mechanical and material characterization of the engineered two-stage resin DIW ink. a) tanδ (dashed) and E' (solid) quantified over a range of temperatures via dynamic mechanical analysis (DMA). b) Features of tensile properties for solely photo cure resin (P), several ratios of photopolymer to epoxy constituents (PE30, PE50, PE70), and solely epoxy resin (E). c) Degree of conversion (DoC) quantified via Fourier transform infrared spectroscopy (FTIR) versus time superimposed over Young's modulus of PE70 resin at 1, 15, 30, and 60 s of UV exposure. d) DoC quantified via FTIR versus time superimposed over Young's modulus of PE70 resin at 0 and 72 h after photo cure.

modulus of 0.915 ± 0.224 MPa, thereby laying the groundwork for layers to retain their deposited shape (Figure 2c). After five seconds of exposure, the network reaches 82% DoC, and is nearly fully developed after 15 s of UV irradiation. As a result, the solidified layers have a Young's modulus of 4.90 ± 0.24 MPa, a 430% increase within 14 s. Based on these results, we elected to expose printed layers to 15 s of UV radiation to assure the printed structures would remain stable during fabrication. It should be noted Young's modulus continues to increase to 7.10 ± 0.80 and 9.86 ± 1.76 MPa for 30 and 60 s exposure, respectively, due to the cumulative UV exposure from curing subsequent layers in fact strengthening prior layers, thus enabling the creation of larger structures. With a modulus of ≈5–10 MPa, the previously printed layer can sustain a large structure without exhibiting visible deformation. For the epoxy resin, FTIR analysis (Figure S2, Supporting Information) revealed that the DoC of the epoxy resin constituent rose to 50% after 24 h, increasing further to 73.2% after 48 h, and finally achieving 86.3% DoC after 72 h in ambient, room-temperature conditions; thereby indicating autonomous network formation behavior under room-temperature conditions (Figure 2d). This curing mechanism proved highly effective in strengthening the material, after 72 h, PE70 resin underwent a three order of magnitude increase in Young's modulus (9.86 MPa to 1.9 GPa) and a two order of magnitude increase in tensile strength (0.79 to 81 MPa) (Figure 2c,d, and S3a,b, Supporting Information).

However, previous studies on extrusion-based 3D printed structures have indicated that mechanical characteristics such as longitudinal and transverse moduli can vary widely. Specifically, depositing material in the direction of tensile loading will result in greater strength than in samples where the material is deposited perpendicular to the direction of loading. To understand and preclude possible characterization inaccuracies in printed structures, we performed tensile experiments using 3D-printed tensile samples comprised of the two-stage resin ink. The first group of samples was deposited in the direction of tensile loading, the second group was printed perpendicular to the direction of loading to examine longitudinal and transverse moduli, and finally samples cast from the same ink batch served as control (Figure S4a–c, Supporting Information).

© 2022 The Authors. Advanced Intelligent Systems published by Wiley-VCH GmbH

The experimental results indicated both longitudinal and transverse sample groups exhibited similar moduli (2.19 ± 0.32 and 2.21 ± 0.12 GPa, respectively), which are comparable to the tensile modulus observed for cast samples using the same print ink (2.1 ± 0.05 GPa) (Figure S4d, Supporting Information). As a result, the moduli of longitudinal and transverse samples exhibited no statistically significant differences (ANOVA, $p = 0.98$).

To confirm the suitability of the two-stage resin ink for DIW 3D printing, we examined viscosity, G', G", and tanδ. Viscoelastic behavior of the hybrid ink was determined via oscillatory stress sweep as shown in Figure S5a, Supporting Information. The ink exhibited a stable plateau of storage modulus G' over loss modulus G", with a value of 2800 Pa and possesses a critical stress (τ_c) of 186 Pa, indicating a high stiffness of the formulated two-stage DIW ink. This is crucial for inverted and horizontal DIW AM to maintain the printed shape versus gravitational sagging post-extrusion. Additionally, we observed that the two-stage resin combined with 7 wt% fumed silica exhibited desirable shear-thinning behavior with respect to viscosity (Figure S5b, Supporting Information). Finally, we conducted an analysis of viscosity versus time to determine an approximate a working life wherein the two-stage ink was reasonably printable (Figure S5c, Supporting Information). Based on the dramatic increase in viscosity at $t = 10\,000$ s, corroborated by qualitative experimental experience, we determined the working life of the two-stage ink to be approximately three hours. This working time allowed for the fabrication of multiple structures, for example, pillar samples used in the following section took approximately 25 min to print.

3.2. Adhesion

To demonstrate the robustness of the two-stage resin bond, and therefore end-use application viability we printed $5 \times 10 \times 20$ mm pillars on several materials (**Figure 3**a). The substrates selected were acrylic, wood, glass, aluminum, and concrete due to their ubiquity in construction and consumer applications. Adhesion strength is quantified by the peak stress (MPa) required to separate the as-printed (with 15 s UV cure) and the fully cured (72 h) printed pillars from the substrates (the test apparatus is shown in Figure 3b). The results of the adhesion experiments are presented in Figure 3c. Printed pillars tested directly after printing exhibited similar adhesion strengths ranging from 0.17 to 0.33 MPa with acrylic substrates exhibiting the lowest adhesion strengths and glass the highest. This range suggests that the photopolymer network can rapidly create a substrate–agnostic bond, indicating that structures of comparable size can be printed in a variety of conditions. Importantly, considering the density of the two-stage resin is 1.2 g cm^{-3}, it is possible to create self-supporting structures up to 28.15 A cm^3 in volume on an acrylic substrate where A is the area of the base of the printed structure in cm^2 (Equation S1, Supporting Information). For example, for the pillar with a 5×10 mm base, the length can be up to 2 m on a wooden substrate. After 72 h, the formation of the epoxy resin matrix doubled and even quintupled in the case of acrylic the adhesion strengths of printed pillars. Indeed, 72 h cure samples, acrylic and wood substrates exhibited the highest adhesion strengths (1.04 ± 0.7 and 0.99 ± 0.7 MPa, respectively). This is potentially due to greater hydrogen bond prevalence caused by hydroxide and ester group interactions

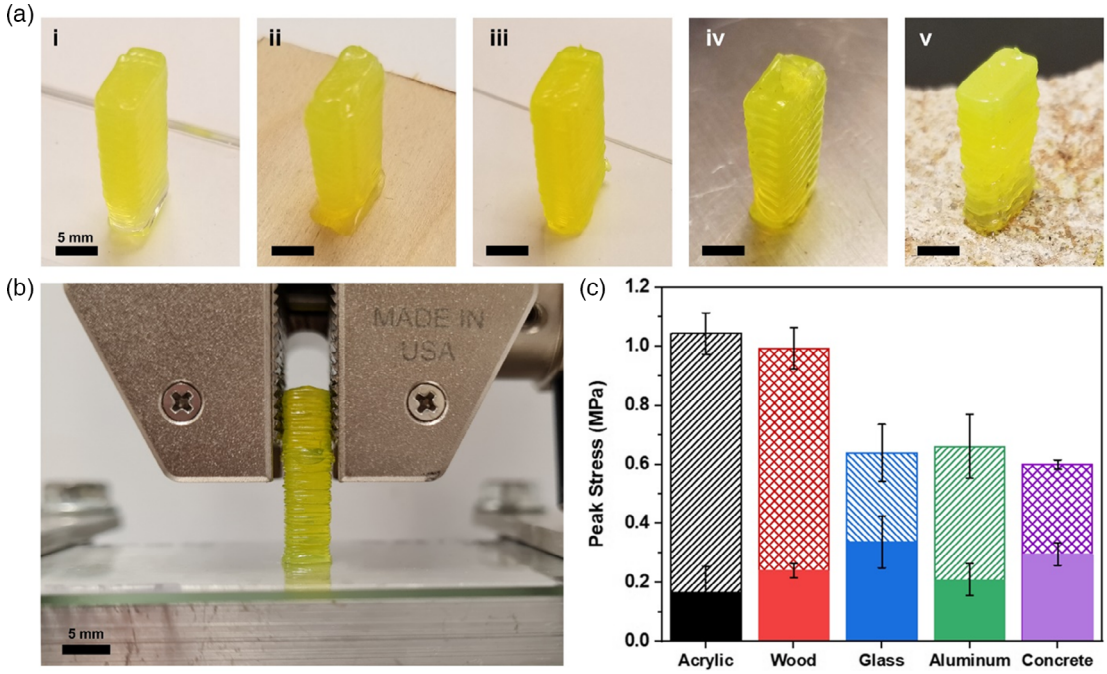

Figure 3. Adhesion strength characterization of DIW printed fully cured two-stage resin structures. a) Two-stage resin structures printed onto: i) acrylic, ii) wood, iii) glass, iv) aluminum, and v) concrete substrates. b) Experimental setup showing the tensile grip clamped to the sample on a fixed substrate. c) Quantified adhesion strengths of printed structures on the aforementioned substrates at 0 h (solid) and 72 h (patterned).

© 2022 The Authors. Advanced Intelligent Systems published by Wiley-VCH GmbH

as well as the surface roughness of wood. Whereas glass, aluminum, and concrete provided similar, lower adhesion strengths (0.64 ± 0.1, 0.66 ± 0.1, and 0.6 ± 0.02 MPa, respectively). The smoothness of the glass and aluminum substrates is a likely contributor to the lower adhesion strength, while failure on the concrete substrate was due to loosened mineral particles at the pillar-substrate interface. Despite these differences, the fully cured printed two-stage resin structures exhibited impressive adhesion strength on a breadth of substrates. As a result, considering the same 5×10 mm base pillar on a wooden substrate, the pillar can grow up to 8 m after four cycles of 72 h curing. These findings further reinforce the importance of the autonomous ambient temperature epoxy curing mechanism for temperature-sensitive substrates such as wood and acrylic.

3.3. Unstructured 3D Printing

To demonstrate the capabilities of our unstructured AM process and two-stage resin, we 3D printed various inverted structures including a bio-inspired "beehive", conical geometries, and load-bearing arches (**Figure 4**a–d, Video S1, Supporting Information). Using the inverted printing technique, we were able to create conical structures with large overhangs without support materials due to a combination of gravitational forces acting "upward" relative to the structure as well as rapid photopolymerization to solidify layers. The synergy of these two phenomena enabled us to create large structures with comparably small base layers without sagging. Furthermore, the multi-phase polymerization mechanism of the printed ink ensured that the large structures preserve their shape integrity over time, thereby ensuring the larger structures continue to resist gravitational forces and do not delaminate from the substrate. To further exemplify the demonstrated overhang printing capabilities coupled with progressive substrate adhesion strength, we printed 24 mm tall arches (Video S2, Supporting Information). Upon fully cured, the arches could support a one-kilogram weight, as corroborated by the adhesion strength characterization previously discussed (Figure 4e). However, the hypothetical strength of this structure is considerably greater. Based on the tensile and adhesion strengths quantified in Figure 2b and 3c, respectively, the tensile strength of the material is at least 85× greater than that of the substrate-structure interface, thus said interface would be the failure location rather than interlayer interfaces. The area of the base of the printed arch is 3.14 cm^2; therefore, an arch printed on an acrylic substrate (adhesion strength = 1.04 ± 0.7 MPa) will have a hypothetical load-bearing capability of 33.23 kg. This is of particular interest when considering the application space of such a structure. To accomplish this feat using conventional DIW manufacturing, the thin-walled structure would likely need to be printed with support material,[32] then removed from the original print substrate and repositioned in an inverted configuration, thereby compromising the bond strength between the structure and end-use surface. Conversely, the proposed unstructured print technique can satisfy this load-bearing task with an as-printed, high-strength structure.

Alternatively, this printing technique can be configured to fabricate structures horizontally, effectively enabling the production of 90° overhangs with zero support material (**Figure 5**a). By reorienting the extrusion nozzle, the zero-support horizontal beams could be fabricated such that layers are deposited parallel to the build plate similar to conventional DIW printing. The rapid photopolymerization affords rigidity to the structure, allowing it to resist the increasing bending moment imparted by the cumulative weight of the horizontal beam. To further demonstrate the capabilities of these unstructured/alternative build orientations, we deposited conductive ink paths on the surface of a horizontally printed beam to create a functional 3D printed structure to

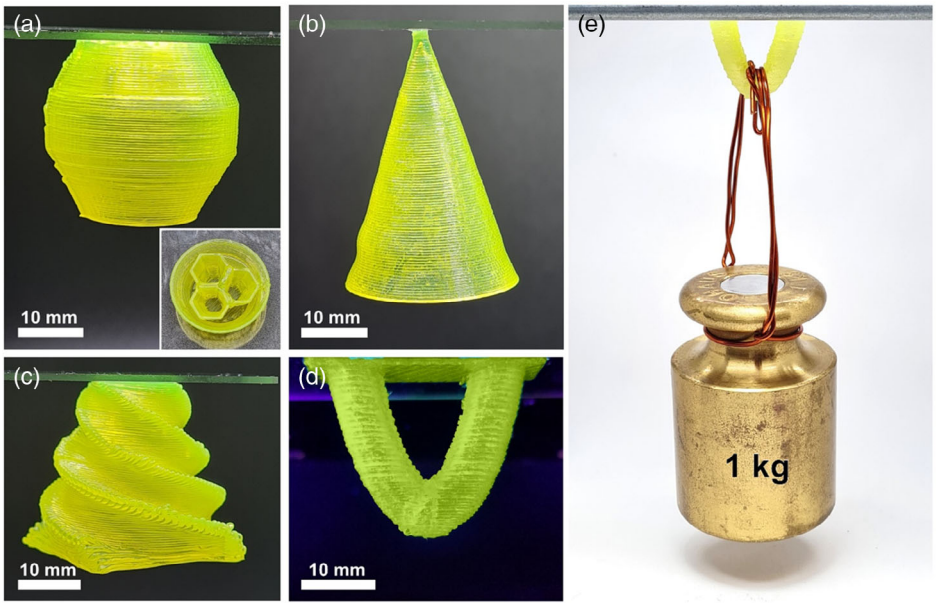

Figure 4. Structures fabricated via the inverted deposition configuration. a) A bio-inspired "beehive". b) Conical structure with large overhangs and small base fabricated with zero support material. c) Twisted conical structure. d) Load-bearing arch. e) Fully cured inverted arch supporting a 1 kg weight.

© 2022 The Authors. Advanced Intelligent Systems published by Wiley-VCH GmbH

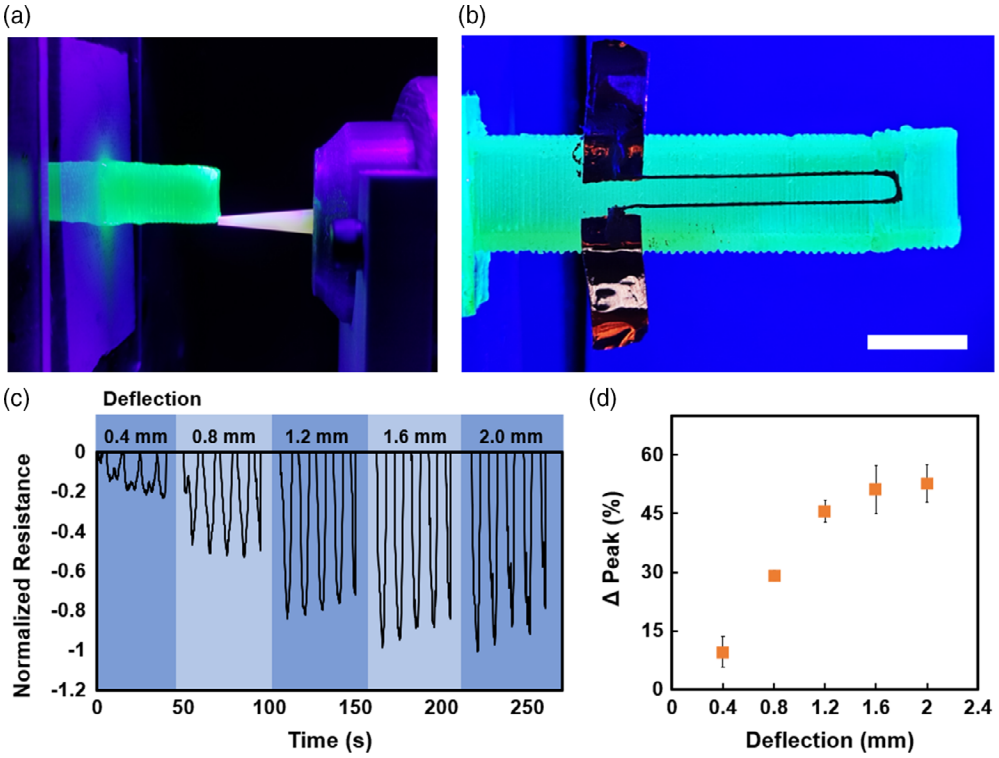

Figure 5. Horizontally printed beam used to create a 3D printed functional structure. a) 3D printing of the horizontal beam. b) The deflection-sensing horizontal beam with DIW deposited conductive path, scale bar = 10 mm. c) Normalized resistance response to 0.4, 0.8, 1.2, 1.6, and 2.0 mm deflections over time. d) Average peak height versus deflection cycling condition.

sense deflection (Figure 5b, Video S3, Supporting Information). The results of normalized resistance over time for the 50 mm horizontal beam sensor subjected to cyclic deflection three times at $\delta = 0.4$, 0.8, and 1.2, 1.6, and 2.0 mm are presented in Figure 5c.

The plotted resistance shows peaks of increasing amplitude in the sensor signal corresponding to prescribed deformation. Indeed, the percent increase from peak to trough of the signal versus deflection shown in Figure 5d indicates a positive trend wherein Δ peak increases from 9.63% to 29.12% for $\delta = 0.4$ and 0.8 mm, respectively. The trend continues finally to 52.74% at $\delta = 2.0$ mm; thereby demonstrating the printed sensor's potential to represent mechanical deformations in the structure. Based on these trends, this printed sensor has the potential to monitor deformations in a pre-existing structure in situ, which could be invaluable in structural health monitoring applications.

4. Conclusions

In this work, we developed a versatile, reconfigurable DIW manufacturing method in tandem with a two-stage hybrid ink designed to facilitate the fabrication of high-strength, self-supporting parts in unconventional printing spaces, such as underneath the build surface or horizontally. Our two-stage hybrid DIW ink combines a photopolymer and tough epoxy resin which is capable of autonomous curing under ambient temperature conditions, thereby creating complex, high-strength geometries without removal of the structure from the printing surface. The photopolymer component can be cured rapidly to enable layer-by-layer fabrication of complex structures. The photocured resin also possesses adequate adhesion to allow the fabrication of large volume structures on a diversity of substrates including acrylic, wood, glass, aluminum, and concrete. Moreover, the epoxy component cured after 72 h in ambient, room-temperature conditions with increased adhesion strengths. We demonstrated the capabilities of the reconfigurable DIW extrusion nozzle method coupled with our developed ink by fabricating complex structures free of support structures in inverted and horizontal environments. The ability to fabricate complex geometries in unstructured environments can be potentially beneficial for printing highly complex parts generated via topology optimization algorithms. In addition, via the addition of DIW-deposited conductive paths, we created a functional 3D printed structure capable of in situ deformation monitoring. These sensing capabilities can be a valuable source of monitoring data to enable the use of machine learning predictive algorithms for maintaining larger structures such as bridges or wind turbines. This work has the potential to be used for applications such as appending new parts to existing structures for increasing functionality, repair, and structure health monitoring.

Supporting Information

Supporting Information is available from the Wiley Online Library or from the author.

© 2022 The Authors. Advanced Intelligent Systems published by Wiley-VCH GmbH

Acknowledgements

C.D.A. and L.Y. contributed equally to this work. H.J.Q. acknowledges the support of AFOSR grants (FA9550- 19-1-0151 and FA9550-20-1-0306; Dr. B.-L. "Les" Lee, Program Manager). H.J.Q. also acknowledges the gift funds from HP, Inc. and Northrop Grumman Corporation. C.D.A. acknowledges the support from Paper Science & Engineering Fellowship.

Conflict of Interest

The authors declare no conflict of interest.

Data Availability Statement

The data that support the findings of this study are available from the corresponding author upon reasonable request.

Keywords

3D printing, additive manufacturing, dual-network polymers, functional structures

Received: July 24, 2022
Revised: September 15, 2022
Published online: October 13, 2022

[1] M. A. H. Khondoker, N. Baheri, D. Sameoto, *3D Print. Addit. Manuf.* **2019**, *6*, 191.
[2] C. D. Armstrong, N. Todd, A. T. Alsharhan, D. I. Bigio, R. D. Sochol, *Adv. Mater. Technol.* **2021**, *6*, 2000829.
[3] M. Lanaro, D. P. Forrestal, S. Scheurer, D. J. Slinger, S. Liao, S. K. Powell, M. A. Woodruff, *J. Food Eng.* **2017**, *215*, 13.
[4] R. Matsuzaki, M. Ueda, M. Namiki, T.-K. Jeong, H. Asahara, K. Horiguchi, T. Nakamura, A. Todoroki, Y. Hirano, *Sci. Rep.* **2016**, *6*, 23058.
[5] C. D. Armstrong, L. Yue, Y. Deng, H. J. Qi, *J. Food Eng.* **2022**, *330*, 111086.
[6] V. C. F. Li, C. K. Dunn, Z. Zhang, Y. Deng, H. J. Qi, *Sci. Rep.* **2017**, *7*, 1.
[7] Q. Fu, E. Saiz, A. P. Tomsia, *Acta Biomater.* **2011**, *7*, 3547.
[8] B. Kim, A. H. Soepriatna, W. Park, H. Moon, A. Cox, J. Zhao, N. S. Gupta, C. H. Park, K. Kim, Y. Jeon, H. Jang, D. R. Kim, H. Lee, K.-S. Lee, C. J. Goergen, C. H. Lee, *Nature Communications* **2021**, *12*, 3710.
[9] D. J. Roach, C. Yuan, X. Kuang, V. C.-F. Li, P. Blake, M. L. Romero, I. Hammel, K. Yu, H. J. Qi, *ACS Appl. Mater. Interfaces* **2019**, *11*, 19514.
[10] V. G. Muir, T. H. Qazi, S. Weintraub, B. O. Torres Maldonado, P. E. Arratia, J. A. Burdick, *Small* **2022**, *18*, 2201115.
[11] X. Peng, S. Wu, X. Sun, L. Yue, S. M. Montgomery, F. Demoly, K. Zhou, R. R. Zhao, H. J. Qi, *Adv. Mater.* **2022**, *34*, 2204890.
[12] L. Friedrich, M. Begley, *J. Colloid Interface Sci.* **2018**, *529*, 599.
[13] M. A. Skylar-Scott, J. Mueller, C. W. Visser, J. A. Lewis, *Nature* **2019**, *575*, 330.
[14] G. J. Cordonier, K. A. Sierros, *ACS Appl. Mater. Interfaces* **2020**, *12*, 15875.
[15] D. Tang, L. Hao, Y. Li, Z. Li, S. Dadbakhsh, *J. Alloys Compd.* **2020**, *814*, 152275.
[16] S. Wu, C. M. Hamel, Q. Ze, F. Yang, H. J. Qi, R. Zhao, *Adv. Intell. Syst.* **2020**, *2*, 2000060.
[17] X. Peng, X. Kuang, D. J. Roach, Y. Wang, C. M. Hamel, C. Lu, H. J. Qi, *Addit. Manuf.* **2021**, *40*, 101911.
[18] Y. Jiang, X. Wang, J. Plog, A. L. Yarin, Y. Pan, *J. Manuf. Processes* **2021**, *69*, 173.
[19] C. Zhou, Y. Yang, J. Wang, Q. Wu, Z. Gu, Y. Zhou, X. Liu, Y. Yang, H. Tang, Q. Ling, L. Wang, J. Zang, *Nat. Commun.* **2021**, *12*, 5072.
[20] C. Ma, S. Wu, Q. Ze, X. Kuang, R. Zhang, H. J. Qi, R. Zhao, *ACS Appl. Mater. Interfaces* **2021**, *13*, 12639.
[21] A. Charlet, F. Bono, E. Amstad, *Chem. Sci.* **2022**, *13*, 3082.
[22] C. Ma, Y. Chang, S. Wu, R. R. Zhao, *ACS Appl. Mater. Interfaces* **2022**, *14*, 33892.
[23] C. Buchanan, L. Gardner, *Eng. Struct.* **2019**, *180*, 332.
[24] L. Li, F. Yu, J. Shi, S. Shen, H. Teng, J. Yang, X. Wang, Q. Jiang, *Sci. Rep.* **2017**, *7*, 9416.
[25] K. Ma, T. Zhao, L. Yang, P. Wang, J. Jin, H. Teng, D. Xia, L. Zhu, L. Li, Q. Jiang, X. Wang, *J. Adv. Res.* **2020**, *23*, 123.
[26] J. A. Lewis, *Adv. Funct. Mater.* **2006**, *16*, 2193.
[27] F. B. Coulter, A. Ianakiev, *3D Print. Addit. Manuf.* **2015**, *2*, 140.
[28] C. Dai, C. C. L. Wang, C. Wu, S. Lefebvre, G. Fang, Y.-J. Liu, *ACM Trans. Graphics* **2018**, *37*, 1.
[29] J. R. Kubalak, A. L. Wicks, C. B. Williams, *Rapid Prototyping J.* **2019**, *25*, 356.
[30] J. Huang, H. O. T. Ware, R. Hai, G. Shao, C. Sun, *Adv. Mater.* **2021**, *33*, 2005672.
[31] J. J. Adams, E. B. Duoss, T. F. Malkowski, M. J. Motala, B. Y. Ahn, R. G. Nuzzo, J. T. Bernhard, J. A. Lewis, *Adv. Mater.* **2011**, *23*, 1335.
[32] S. K. Romberg, A. I. Abir, C. J. Hershey, V. Kunc, B. G. Compton, *Addit. Manuf.* **2022**, *53*, 102677.
[33] X. Song, Y. Pan, Y. Chen, *J. Manuf. Sci. Eng.* **2015**, *137*, 021005.
[34] T. Wu, P. Jiang, X. Zhang, Y. Guo, Z. Ji, X. Jia, X. Wang, F. Zhou, W. Liu, *Mater. Des.* **2019**, *180*, 107947.
[35] X. Kuang, Z. Zhao, K. Chen, D. Fang, G. Kang, H. J. Qi, *Macromol. Rapid Commun.* **2018**, *39*, 1700809.
[36] D. J. Roach, C. M. Hamel, C. K. Dunn, M. V. Johnson, X. Kuang, H. J. Qi, *Addit. Manuf.* **2019**, *29*, 100819.
[37] C. D. Armstrong, L. Yue, X. Kuang, D. J. Roach, M. L. Dunn, H. J. Qi, *J. Compos. Mater.* **2022**, 002199832211192.

© 2022 The Authors. Advanced Intelligent Systems published by Wiley-VCH GmbH